Current Biology 23, 515–522, March 18, 2013 ©2013 Elsevier Ltd All rights reserved http://dx.doi.org/10.1016/j.cub.2013.02.013

Report

Near-Real-Time Feature-Selective Modulations in Human Cortex

Javier O. Garcia,[1,*] Ramesh Srinivasan,[3] and John T. Serences[1,2,*]
[1]Department of Psychology
[2]Neuroscience Graduate Program
University of California, San Diego, La Jolla, CA 92093-0109, USA
[3]Department of Cognitive Sciences, University of California, Irvine, Irvine, CA 92697-5100, USA

Summary

For neural activity to be linked with cognitive function, information is needed about both the temporal dynamics and the content of neural codes. Traditionally, recording of single neurons in animals has been the primary means of obtaining high temporal resolution and precise information about neural tuning properties such as selectivity for different sensory features. Recent functional magnetic resonance imaging (fMRI) studies in humans have been able to measure feature selectivity within specific subregions of sensory cortex (e.g., orientation selectivity in primary visual cortex, or V1) [1, 2]. However, investigating the neural mechanisms that support cognitive processing—which often occurs rapidly on a subsecond scale—with a temporally insensitive method such as fMRI severely limits the types of inferences that can be drawn. Here, we describe a new method for tracking the rapid temporal evolution of feature-selective information processing with scalp recordings of electroencephalography (EEG). We generate orientation-selective response profiles based on the spatially distributed pattern of steady-state visual evoked potential (SSVEP) responses to flickering visual stimuli. Using this approach, we report a multiplicative attentional modulation of these feature-selective response profiles with a temporal resolution of 24–120 ms, which is far faster than that achieved with fMRI. Finally, we show that behavioral performance on a discrimination task can be predicted based on the amplitude of these temporally precise feature-selective response profiles. This method thus provides a high-temporal-resolution metric that can be used to track the influence of cognitive manipulations on feature-selective information processing in human cortex.

Results and Discussion

Sensory systems operate via the joint activity of millions of neurons that are tuned to different stimulus attributes, and the tuning of these neurons becomes increasingly complex as information is relayed through successive stages of processing [3, 4]. For example, many neurons in the retina respond most strongly to small spots of light, many neurons in early areas of visual cortex (e.g., primary visual cortex) respond most strongly to oriented lines, and neurons at later stages of visual cortex respond most strongly to complex objects such as faces [5, 6]. As a result of this neural selectivity and the fact that decisions based on sensory inputs can often be made in hundreds of milliseconds, understanding the computational principles that underlie neural information processing requires both sensitivity to the stimulus attributes being processed (feature selectivity) and high temporal resolution. Over the last several decades, electroencephalography (EEG) and magnetoencephalography (MEG) have primarily been used to achieve a high temporal resolution [e.g., 7–9], whereas functional magnetic resonance imaging (fMRI) has been used to achieve a high degree of feature selectivity [e.g., 10–12]. However, few studies have attempted to make inferences at both levels of analysis, thus limiting our understanding of information processing in human cortex.

Recently, many studies have exploited changes in multivariate patterns of activation across fMRI images to recover feature-selective responses in human visual cortex (multivariate pattern analysis, or MVPA, methods) [1, 11–14]. For instance, fluctuations in activation patterns within early visual areas can be used to predict the specific orientation of a stimulus being viewed by a subject [1, 15]. The systematic orientation-dependent modulation of voxel responses within these early visual areas is thought to be driven by small modulations in neural activity at the columnar level (~300–500 μm) [1, 16] and by modulations across larger-scale maps of orientation that are arrayed across early areas of the visual system such as V1 [17].

These relatively new multivariate approaches to fMRI analysis fall into two broad categories. *Decoding* analyses use pattern recognition techniques to estimate which specific stimulus—selected from a larger set of possible stimuli—was most likely to have been viewed based on an observed pattern of activation. To the extent that these algorithms can correctly guess the stimulus label, one can infer that some stimulus-specific information is being encoded in the cortical region of interest [11–13, 18]. However, while decoding analyses are very sensitive to changes in the information content of a cortical area, they do not directly reveal *how* changes in patterns of neural activity give rise to separable activation patterns at the macroscopic level afforded by fMRI. Thus, to complement decoding models, recent studies have employed *encoding* models that use a priori assumptions about different feature spaces—such as the well-known orientation selectivity of neurons in primary visual cortex [19, 20]—to make inferences about how experimental manipulations change population-level neural response profiles. These forward encoding models have been used to reconstruct novel visual stimuli [21], to investigate color- and orientation-selective responses in early visual cortex [2, 22, 23], and to examine the effects of feature-based attention on the shape of orientation selective response profiles in primary visual cortex [24].

Despite these advances, BOLD neuroimaging has inherently poor temporal resolution on the order of several seconds and can subsequently reveal little about the dynamics of neural information processing. Here, we combine decoding and encoding models with EEG to determine whether

*Correspondence: javiergarcia@ucsd.edu (J.O.G.), jserences@ucsd.edu (J.T.S.)

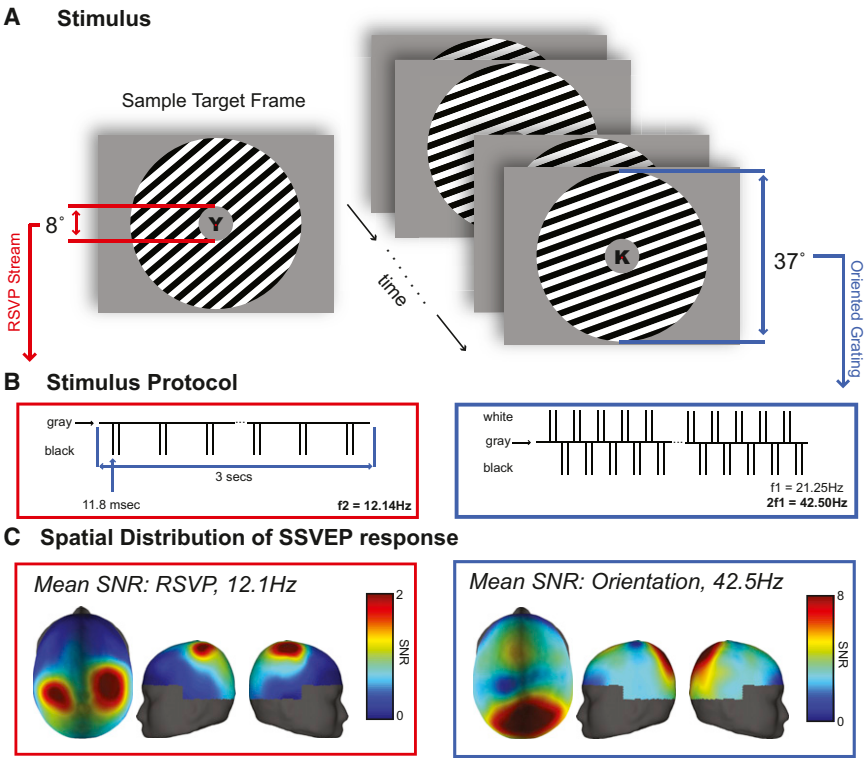

Figure 1. Stimulus Protocol and SSVEP Response

(A) Stimulus display: In the central location, a stream of letters was simultaneously presented with an oriented peripheral annulus on a uniform gray background. During the 3,000 ms trial, a target would appear as a shift in the orientation of the grating or an X or Y in the RSVP stream of letters. Subjects responded with a button press to the direction of the shift (clockwise/counterclockwise) or to the target letter (X orY).

(B) Stimulus protocol: Stimuli were tagged with different flicker frequencies. The annulus was contrast reversed at 21.25 Hz, and the RSVP stream of letters was updated at rate of 12.1 Hz (50% duty cycle).

(C) Mean of the SNR across subjects of the SSVEP responses to the flickering stimuli, calculated by dividing the power at the stimulus frequency (or the second harmonic of the stimulus frequency for the peripheral grating, see the Experimental Procedures) by the standard deviation of the surrounding frequencies, 6.7 Hz on each side of the stimulus frequency). Spatial distributions reflect a parietaloccipital response for the grating stimulus and a bilateral parietal response for the RSVP stimulus.

See also Figure S5.

more-precise temporal information can be recovered about feature-selective modulations in human cortex and whether any observed feature-selective modulations are sensitive to task demands. To this end, we designed a behavioral task to examine orientation-selective responses under conditions of focused or withdrawn attention. Subjects viewed a visual display containing a square-wave-oriented grating rendered in a large circular annulus and a rapid serial visual presentation (RSVP) stream of letters that was presented within the annulus at fixation (Figures 1A and 1B). On half of the trials, subjects attended the peripheral grating and pressed a button when they detected a clockwise (CW) or a counterclockwise (CCW) shift in the orientation of the grating. On the other half of the trials, subjects ignored the peripheral grating and pressed a button whenever they detected a prespecified target letter in the central RSVP stream. To delineate neural responses separately for each stimulus (grating versus RSVP stream), we *tagged* stimuli with different flicker frequencies: the contrast of the peripheral grating was reversed at 21.25 Hz, and the RSVP stream of letters was updated at a rate of 12.1 Hz. Steady-state visual evoked potentials (SSVEPs) were estimated with a Fourier analysis to separately assess the response to each stimulus. We focused our analyses on the magnitude of the second harmonic of the flickering grating (42.5 Hz) and the magnitude of first harmonic of the flickering RSVP stream, consistent with known differences in contrast-reversed and luminance-defined SSVEPs (see Figure 3A for full spectra and stimulus related activity across time) [25]. The dominant response at twice the reversal frequency (42.5 Hz) of the orientation grating elicited a focal response with a peak over the parietal-occipital region. Peak average responses span from electrodes corresponding to POz to Pz (posterior to anterior) and P1 to PO4 (left to right), with largest amplitude centered at Pz (in descending signal-to-noise ratio [SNR]: Pz, PO4, POz, P2, and P1). The 12.1 Hz response to the RSVP stream, however, had a bilateral spatial distribution with peaks in parietal cortex (Figure 1C).

We first used a linear classifier to determine whether stimulus orientation could be decoded on the basis of the spatial distribution of the SNR and the phase of the SSVEP response at 42.5Hz across selected electrodes (see the Supplemental Experimental Procedures, "SSVEP Responses," available online). Classification accuracy for orientation was significantly above chance even when subjects were attending to the central RSVP stream (blue bars in Figure 2A; $p < 0.05$; note that this and all other p values computed via a bootstrapping procedure; see the Supplemental Experimental Procedures and Figure S4). Moreover, classification accuracy increased significantly when subjects attended to the oriented grating, demonstrating that the orientation selective patterns of SSVEP were sensitive to task demands ($p < 0.05$; Figure 2A). In contrast, the power and phase of the SSVEP responses evoked by the RSVP stream (12.1 Hz) could not be used to decode the orientation of the stimulus (red bars in Figure 2A; $p > 0.05$). The EEG electrodes that contained the highest SNR were also the most diagnostic for this analysis (Figure 2B).

Having established that the spatial distribution of SSVEP power and phase can be used to successfully *decode* the angle of the orientated grating, we next considered whether the power and phase could also be used to reconstruct a population-level representation of the orientation-selective neural activity (i.e., a population-level orientation tuning function, or TF). We used a linear forward encoding model that has been previously used to estimate feature-selective tuning functions using fMRI [2, 22, 26, 27]. In short, we estimated the magnitude of the response in each electrode as a linearly weighted sum

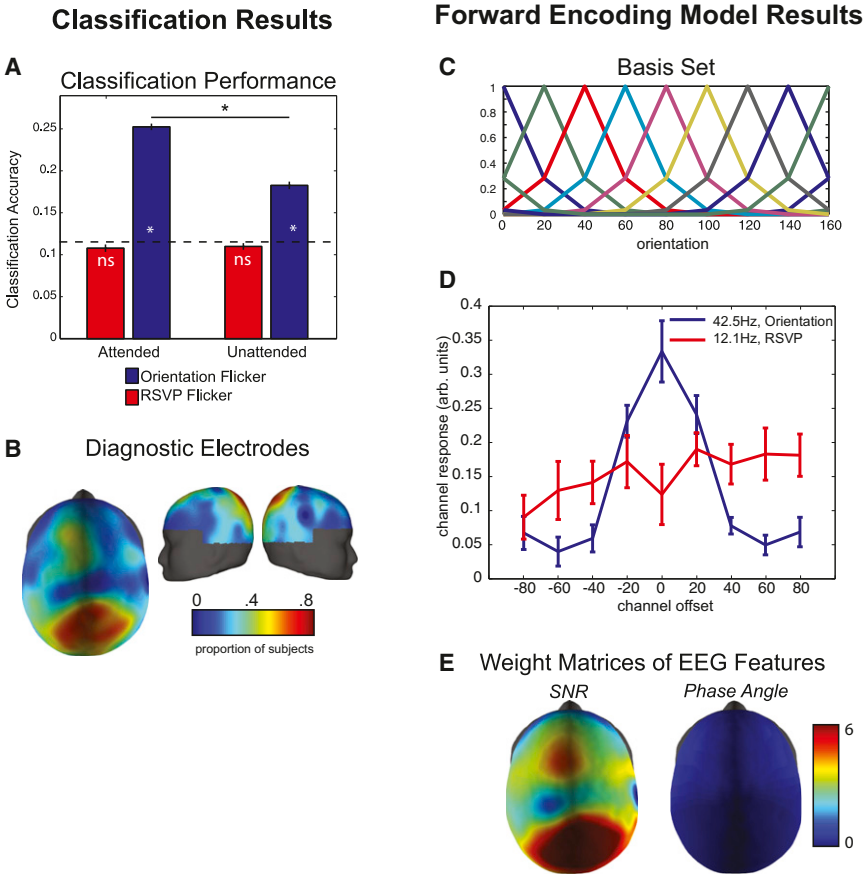

Figure 2. Decoding and Encoding Orientation from the SSVEP Response

(A) Linear discriminant classification results. For each subject, the SNR and phase of a subset of electrodes elements was used for the classification procedure, and the peak of the classification function was used as that subject's classification performance (see Figure S4 and the Supplemental Experimental Procedures). The orientation of the grating could be decoded above chance ($p < 0.05$) based on the SSVEP response at 42.5 Hz (Figure 2A, blue bars), and decoding accuracy was higher when the grating was attended compared to when it was not attended. In contrast, the orientation of the peripheral grating could not be decoded based on the SSVEP response at 12.1Hz (red bars). The dotted line represents chance performance in this nine-way classification, and error bars represent the SEM across subjects. Asterisks indicate significant differences via a bootstrap procedure (see the Supplemental Experimental Procedures).

(B) Diagnostic electrodes in the linear discriminant analysis across subjects: the color map of the topographic plot shows the probability that an electrode was used in the decoding analysis. The electrodes that contained the highest SNR (Figure 1C) were also the most diagnostic.

(C) Basis set used in the forward encoding model, derived from half-sinusoidal functions raised to the sixth power (nine basis functions spanning 0°–160° in 20° steps).

(D) Dynamic tuning functions derived using the forward encoding model based on SNR and phase angle of the SSVEP response before the target onset. The 12.1 Hz SSVEP response to the RSVP flicker does not produce tuned responses whereas the 42.5 Hz SSVEP response produces a tuned response that peaks at the angle of stimulus being viewed (which is 0° in this plot by convention). Error bars represent the SEM across subjects.

(E) Average weight of the maximum channel response showing that the SNR of the parietal-occipital electrodes and, to a lesser extent the phase angle of the frontal electrodes, carries most of the orientation-selective information.

See also Figures S4 and S7.

of the idealized orientation tuning functions shown in Figure 2C. Using these weights, we then estimated the relative magnitude of the SSVEP response within different subpopulations of neurons (or "channels") that are tuned to different orientations (see the Experimental Procedures).

We first established the effectiveness of this technique when applied to the power and phase of the SSVEP response at 42.5 Hz based on a Fourier analysis of the data from the entire interval before the onset of the target. Only data collected prior to target onset were used, to avoid contamination by responses to the rotation of the grating either CW or CCW. The enhanced response to neural populations tuned to the orientation of the stimulus being viewed, accompanied by the characteristic Gaussian dropoff in the signal associated with neural populations tuned successively farther away, demonstrates that SSVEP power and phase can be used to estimate the shape of feature-selective population response profiles in human cortex (Figure 2D). Moreover, projection of the data from electrode space into orientation channel space does not significantly degrade the amount of orientation-selective information, as linear classification performed on single trial tuning functions is well above chance (21.8% collapsed across all conditions).

We next examined the extent to which each electrode contributed to these feature-selective population TFs. Perhaps not surprisingly based on the SNR plots in Figure 1C, power fluctuations in a relatively focal set of occipital-parietal electrodes carried most of the orientation-selective information (Figure 2E). The orientation-selective modulation of phase, on the other hand, was most evident in electrodes over frontal cortex; however, phase contributed far less information to the orientation-selective TFs shown in Figure 2E (see also Figure S1A).

As a control analysis, we also attempted to generate orientation-selective TFs based on the power and phase of the SSVEPs associated with the RSVP stream (12.1 Hz). We were not able to compute feature-selective TFs on the basis of the response associated with the RSVP stream, irrespective of whether the subject was attending the RSVP stream or the peripheral grating. Thus, the feature-selective population response profiles shown in Figure 2 are specific to the neural response associated with the flickering grating. Finally, we also inspected individual electrode tuning functions (Figure S1B) and noted fluctuations in each electrode as a function of stimulus orientation with no substantial changes in overall mean response amplitude. This implies that feature selectivity is driven by aggregation of weak orientation selective signals across electrodes.

As the data presented thus far relied on the power and phase of the SSVEPs across a large time window (the entire pretarget

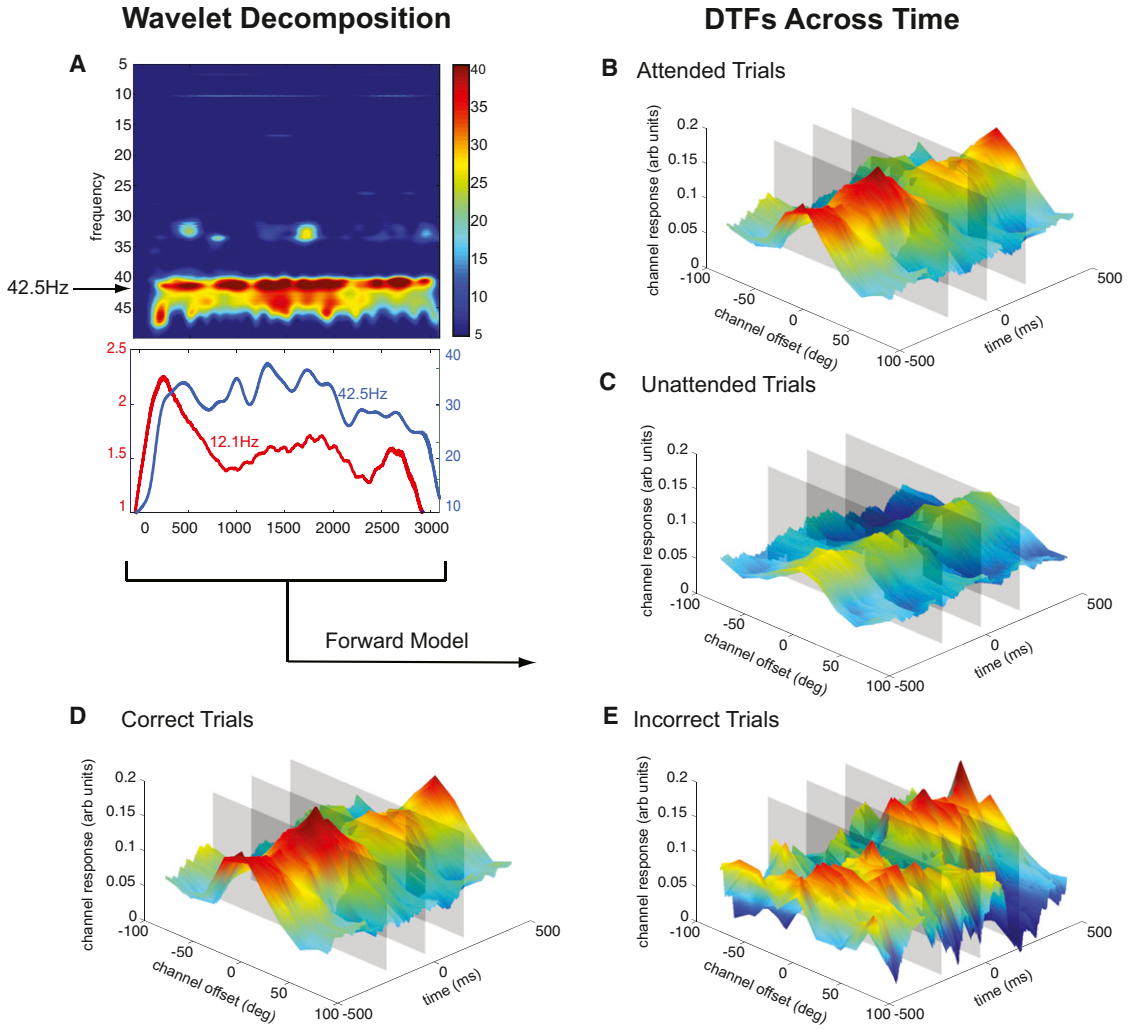

Figure 3. Dynamic Tuning Functions

(A) A wavelet decomposition of frequencies 5–50 Hz averaged across subjects and conditions. The lower plot shows a line plot of stimulus related responses (RSVP stream, 12.1Hz; oriented grating, 42.5Hz).

(B–E) Forward encoding model results derived from a wavelet decomposition of the SSVEP response. With SNR and phase angle of the SSVEP response, locked to the target onset (500 ms before to 500 ms after), orientation response profiles were reconstructed as a function of time. Segregating trial types reveals differences between responses to attended stimuli (B) and unattended stimuli (C) and between correct trials (D) and incorrect trials (E). Gray planes mark time points of interest (200 ms before target onset, target onset, and target termination; see Figure 4).

See also Figures S1–S3, S6, and S7.

window), we next evaluated the temporal precision with which we could measure orientation-selective response profiles. We used a wavelet that was progressively shifted across time in 1 ms intervals to compute the power and phase of the SSVEP response at 42.5 Hz (Figure 3A). Note that even though we sampled at 1,000 Hz, the smallest meaningful unit of time in this study is one stimulus cycle, or 24 ms, which provides the upper limit on our temporal resolution. Moreover, the Gaussian window of the wavelet effectively averages over a slightly larger temporal window spanning five cycles of the flickering grating (or 120 ms). Thus, the temporal resolution is between 24 ms and 120 ms and will vary as a function of the temporal bandwidth of the Gaussian envelope and the flicker frequency of the stimulus.

This analysis revealed dynamic TFs (DTFs) that were sensitive to both behavioral performance and task demands (Figure 3). For example, these DTFs reveal a sustained multiplicative increase in amplitude when subjects were attending to the peripheral grating compared to when they were attending to the central RSVP stream (Figures 3B and 3C). Moreover, during trials in which the peripheral grating was attended, the DTFs were significantly higher in the pretarget interval on correct compared to incorrect trials (Figures 3D, 3E, and 4C). This increase in the gain of the DTFs on correct trials is apparent across the entire 500 ms interval before target onset. We confirmed these effects were not driven by the fact that an error was made on only ~20% of all trials by observing the same effect when we randomly sampled subsets of the correct trials (Figure S2).

A closer inspection of the DTFs derived from correct trials also reveals rapid changes in the magnitude of the response profiles immediately before and after the target onset (Figure 4). To characterize the differences between the conditions, we inspected DTFs across a 200 ms window before the onset

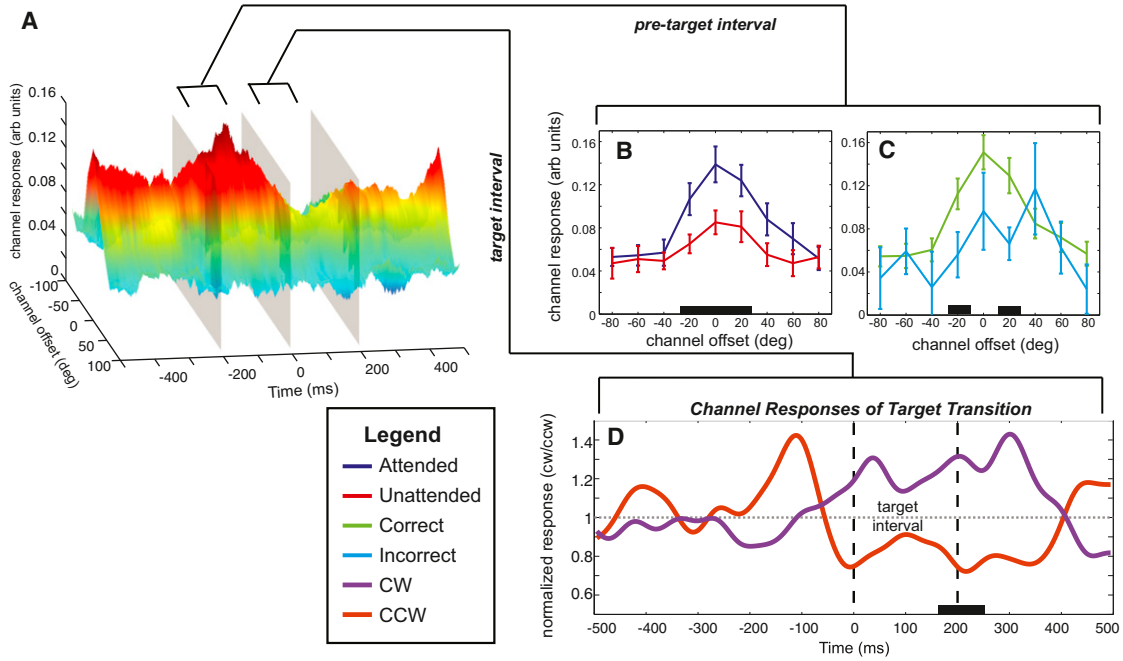

Figure 4. Dynamics of Reconstructed Orientation Channel Responses

(A–C) Rotated view of Figure 3D (correct attended trials) (A). Each inset line plot shows the tuning functions derived from the time window 200 ms before target onset (B and C). These line plots display the effect of attention (B) and the effect of accuracy (C). Error bars represent the SEM across subjects, and significant differences between channel responses indicated by black bars on the x axis.

(D) Normalized response in channels tuned 20° and −20°) separated by clockwise or counterclockwise target shifts. These responses show a shift in the response beginning 60 ms before target onset extending 400 ms after target onset. Significant divergence occurs between 165 and 255 ms after target onset (black bar on x axis).

of the target (Figure 4B). When subjects were attending to the oriented grating, the pretarget interval shows a significantly larger response at −20°, 0°, and 20° channel offsets on attended compared to unattended trials. In Figure 4C, we compare correct and incorrect trials (of only attend-grating trials). The difference between correct and incorrect trials is most reliable at −20° and 20° channel offsets (also visible at 0°) within the pretarget interval. Furthermore, the orientation shift of the grating (the appearance of the target) is visible in the channel responses across time. Figure 4D displays the normalized response in the −20° and 20° channels to both clockwise and counter-clockwise targets. The divergence in responses occurs approximately 60 ms before the target onset and extends to 200 ms after the termination of the target. Presumably, the onset of this separation before the onset of the target is related to the 120 ms temporal envelope of the wavelet filter that was used to derive the SSVEP response. However, note that the responses are significantly different only 165–255 ms after the target onset ($p < 0.05$), highlighting the high temporal precision of this technique.

Previous electrophysiological studies have examined the time course of evoked signals when subjects are instructed to attend to specific visual features [e.g., 7, 8, 28–30]. While these studies show that feature-based attention can mediate evoked responses as early as 90 ms after stimulus [8], none of these studies examined how attention shapes feature-selective population response profiles across time. In addition, EEG/MEG activity patterns have been used to infer, or decode, which stimulus feature a subject is viewing [31, 32]. However, they did not examine the influence of cognitive manipulations on the information content of activity patterns, and decoding methods cannot be easily used to infer how the shape of feature-selective response profiles changes with task demands. This is a key advantage of the current approach, as understanding the influence of cognitive demands on information processing in human cortex requires examining *how* the response profile across feature-selective neurons changes over time [33]. In turn, the lack of real-time information about the effects of attention on feature-selective responses in human cortex has contributed to a long-standing debate about the nature of attentional modulation and how it might differ in monkey and man. For instance, previous single-unit recording studies have reported that attention primarily operates via a multiplicative scaling of neural TFs [e.g., 34, 35]. In contrast, fMRI studies have shown that attention primarily induces an additive shift and that multiplicative gain is relatively weak in comparison [24, 36–38]. The dominance of additive effects in fMRI might reflect the fact that the BOLD response pools responses across a large number of neurons that probably exhibit different degrees of feature selectivity and attentional modulation. Thus, the aggregate response might look additive as opposed to multiplicative. However, the fact that we see a modulation pattern that more closely resembles the multiplicative scaling observed with single-unit recording (Figure 4B), despite the fact that EEG also pools across the responses of large numbers of neurons, suggests instead that BOLD fMRI might be indexing a fundamentally different source of modulation. In addition, the tight correspondence between single-unit recordings and the present DTFs is also encouraging, because human subjects can learn complex new experimental paradigms very quickly compared to nonhuman primates, who often require months of training to

successfully perform relatively simple tasks. Thus, the present technique might be used to evaluate information processing in a wide variety of experimental settings and in a manner that is not influenced by long-term learning effects that might alter the nature of neural activity across the course of months of training.

As EEG has relatively coarse spatial resolution, it is difficult to make a precise statement about the exact cortical area that is driving these feature-selective DTFs (e.g., V1, V2, etc.). Our EEG signals reflect synaptic activity synchronized to an external signal (stimulus flicker) but space-averaged on the centimeter scale. In order to focus on early visual areas (rather than parietal or even frontal activity), we specifically entrained EEG signals related to the oriented grating at a high frequency based on the logic of coupled oscillators [e.g., 39]. This framework asserts that only small local networks can operate at high frequencies, whereas larger networks operate at lower frequencies due to transmission delays along axonal fiber systems. Indeed, in another study, the use of lower frequency flicker engages parietal and frontal networks, whose properties are expected to be less closely related to the physical stimulus features and more closely related to attentional goals [40]. In addition, we observe a tight phase coupling at 42.5 Hz across all of the high SNR electrodes, which is consistent with a single cortical source driving the SSVEP response to the flickering grating (whereas multiple sources should give rise to a phase shift between electrodes; see Figure S5). However, even if we are reasonably confident that our SSVEP signals originate from a single source in occipital cortex, the spatial scale of the orientation signals is still not clear. Indeed, the origin of orientation-selective signals measured with other methods such as fMRI is still a matter of active debate. Some researchers propose that orientation-selective response biases are linked to subtle imbalances in the distribution of orientation selective columns within each voxel [1, 41]. In contrast, others have reported a spatial correspondence between large-scale orientation maps and polar angle maps that were identified via standard retinotopic mapping methods [17]. Although it is likely that both sources of information contribute to orientation-selective fMRI responses, the existence of large-scale orientation information that spans primary visual cortex should give rise to signals that are capable of driving robust changes in the spatial distribution of SSVEPs. However, this conclusion should be qualified because we cannot rule out contributions from other sources given the limited spatial resolution of the present method. In either case, the present experiment establishes that orientation-selective responses detected with SSVEP provide a useful index to link neural and cognitive levels of information processing.

In sum, the temporal resolution provided by SSVEPs provides a unique method for measuring brain function and has been previously used to study several distinct cognitive phenomena [9, 42, 43]. Here we exploit the continuous nature of the oscillatory activity elicited by a flickering stimulus and demonstrate that relatively simple models can be used to reconstruct temporally precise orientation-selective response profiles from the distributed pattern of the power and phase of evoked electrical activity across the scalp. This ability is primarily supported by small orientation-selective changes in power across a relatively focal set of occipital-parietal electrodes, with a smaller additional contribution from the phase angle across electrodes in frontal cortex. Importantly, these feature selective response profiles provide high temporal and high featural resolution and are modulated by both task demands (attention) and behavioral performance. These latter demonstrations establish that the tuning functions reflect active cognitive processing and also extend previous single-unit physiology work by linking feature-based attentional modulations with behavior. Compared to fMRI, the spatial resolution of EEG is quite coarse; however, the high temporal resolution and the feature selectivity that we report here represents a significant advance over previous applications of EEG and provides a near real-time index of neural information processing from human cortex.

Experimental Procedures

Sixteen individuals (eight female) participated in the experiment, and all data was collected at the Perception and Cognition Lab at the University of California, San Diego (UCSD). All participants provided written informed consent in accordance with the human subjects Institutional Review Board at UCSD. EEG measurements were collected with a dense array NetAmps 300 system made by EGI (Electrical Geodesics, Eugene, OR) equipped with a 128 channel Hydrocel Geodesic Sensor Net and a photocell system to give accurate and fast sampling of each cycle of the stimulus. The EEG was recorded with a 1,000 Hz sampling rate. Stimuli consisted of a square-wave grating that was rendered in a circular annulus (37° diameter visual angle) with a central fixation dot (0.4° visual angle) on which subjects were required to maintain gaze (Figure 1). A rapid serial visual presentation (RSVP) stream of letters (8° visual angle) was simultaneously presented at the center of the screen. For delineation of neural responses separately for each stimulus (grating versus RSVP stream), stimuli were *tagged* with different flicker frequencies: the annulus was contrast reversed at 21.25 Hz, and the RSVP stream of letters was updated at rate of 12.1 Hz (50% duty cycle). Stimuli were presented on a uniform gray background (43.2 cd/m^2) with a monitor refresh rate of 85 Hz. For "attend grating" blocks of trials, subjects maintained fixation and attended to the oriented grating (grating rendered in one of nine possible orientations across trials, 0°–160° in steps of 20°). At some point during each 3,000 ms trial, the orientation of the grating would rotate either clockwise or counterclockwise for 235 ms (20 frames), and subjects would report the direction of angular shift with a button press after the end of each trial. Using the method of constant stimuli, performance at six orientation deviations was obtained. For the "attend RSVP" blocks of trials, subjects maintained fixation while attending to the central letter stream. Subjects were instructed to respond to a target letter (X or Y) with a button press after the end of each trial. We adjusted the angular offset of the grating target and the contrast of the letters in a pre-experiment training session to ensure that accuracy on both tasks was ~80% (see the Supplemental Experimental Procedures). To maximize stimulus related activity in the EEG and to ensure that the subjects attended the stimulus for an extended period of time, 80% of the targets were presented 2,000 ms or more after the onset of the stimulus.

Each block lasted for approximately 7 min and contained 90 trials (ten trials for each of the nine orientations). Four blocks were run for each of the attention conditions, which took about 1 hr and yielded 360 trials for each condition (720 total). After standard artifact editing procedures (eye-blink correction, trial rejection, etc.; see the Supplemental Experimental Procedures) each individual trial was cropped to an integer number of cycles to maximize a narrow band stimulus response. Trials were then Fourier transformed with conventional FFT methods via Matlab and normalized based on a prestimulus period of 100 ms.

Decoding was conducted via a linear discriminant analysis to determine whether the orientation of the stimulus could be predicted from the SSVEP response. The number of electrodes included in the classification procedure varied across subjects (see the Supplemental Experimental Procedures section entitled "Classification Analysis" and Figure S4). The forward encoding model used to generate orientation tuning functions used a method that was similar to previous fMRI studies developed by Brouwer and Heeger [2, 22, 24, 26]. In brief, let m be the number of EEG elements for an individual subject's data set and n_1 be the number of trials in the training set (719 trials) and n_2 be the number of observations in the testing set (one trial). Finally, let k be the number of hypothetical orientation channels (C_1, $k \times n_1$), composed of half-sinusoidal functions raised to the sixth power as the basis set. Let B_1 ($k \times n_1$) be the training set and B_2 ($k \times n_2$) be the test set. The training data in

B1 were then mapped onto the matrix of channel outputs (C1) by the weight matrix (W, *m x k*) that was estimated with a GLM of the form

$$B_1 = WC_1, \quad (1)$$

where the ordinary least-squares estimate of W is computed as

$$\widehat{W} = B_1 C_1^T \left(C_1 \, C_1^T \right)^{-1}. \quad (2)$$

The channel responses C_2 (k x n_2) were then estimated based on the test data (B_2) with the weights estimated in (2):

$$\widehat{C}_2 = \left(\widehat{W}^T \widehat{W} \right)^{-1} \widehat{W}^T B_2. \quad (3)$$

This process was then repeated by holding of each trial out in turn until all trials had served as a test set. Then the channel response function on each trial was circularly shifted to a common stimulus-centered reference frame, and these recentered response functions were averaged across conditions of interest (e.g., attend grating and attend RSVP stream). Thus, by convention, the 0° point along the x axis in all plots refers to the orientation of the stimulus that evoked the response profile. The number of EEG elements used for each subject varied slightly across subjects depending just on the number of artifact-free channels (average of 238 elements, 119 SNR, and 119 phase angle estimates).

For the creation of DTFs, a separate training/test procedure was run on the power and phase of the SSVEP response at each time point as estimated using a continuous wavelet transform. After this procedure, the channel responses were locked to the target onset (Figures 3 and 4). The significance of all of the effects was assessed with a bootstrap procedure and an alpha level of 0.05. Methods are described in more detail in the Supplemental Experimental Procedures.

Supplemental Information

Supplemental Information includes seven figures and Supplemental Experimental Procedures and can be found with this article online at http://dx.doi.org/10.1016/j.cub.2013.02.013.

Acknowledgments

This work was supported by NIH RO1-068004 to R.S. and by NIH RO1-092345 to J.T.S. We thank Candace Linscheid and Danna Lee for assistance in data collection, Edward Awh for input on early versions of this research project, and Kimberly Kaye for useful discussions.

Received: October 23, 2012
Revised: January 14, 2013
Accepted: February 7, 2013
Published: March 7, 2013

References

1. Kamitani, Y., and Tong, F. (2005). Decoding the visual and subjective contents of the human brain. Nat. Neurosci. *8*, 679–685.
2. Brouwer, G.J., and Heeger, D.J. (2011). Cross-orientation suppression in human visual cortex. J. Neurophysiol. *106*, 2108–2119.
3. Riesenhuber, M., and Poggio, T. (1999). Hierarchical models of object recognition in cortex. Nat. Neurosci. *2*, 1019–1025.
4. Kobatake, E., and Tanaka, K. (1994). Neuronal selectivities to complex object features in the ventral visual pathway of the macaque cerebral cortex. J. Neurophysiol. *71*, 856–867.
5. Grill-Spector, K., and Malach, R. (2004). The human visual cortex. Annu. Rev. Neurosci. *27*, 649–677.
6. DiCarlo, J.J., Zoccolan, D., and Rust, N.C. (2012). How does the brain solve visual object recognition? Neuron *73*, 415–434.
7. Zhang, W., and Luck, S.J. (2009). Feature-based attention modulates feedforward visual processing. Nat. Neurosci. *12*, 24–25.
8. Schoenfeld, M.A., Hopf, J.M., Martinez, A., Mai, H.M., Sattler, C., Gasde, A., Heinze, H.J., and Hillyard, S.A. (2007). Spatio-temporal analysis of feature-based attention. Cereb. Cortex *17*, 2468–2477.
9. Andersen, S.K., and Müller, M.M. (2010). Behavioral performance follows the time course of neural facilitation and suppression during cued shifts of feature-selective attention. Proc. Natl. Acad. Sci. USA *107*, 13878–13882.
10. Naselaris, T., Kay, K.N., Nishimoto, S., and Gallant, J.L. (2011). Encoding and decoding in fMRI. Neuroimage *56*, 400–410.
11. Tong, F., and Pratte, M.S. (2012). Decoding patterns of human brain activity. Annu. Rev. Psychol. *63*, 483–509.
12. Serences, J.T., and Saproo, S. (2012). Computational advances towards linking BOLD and behavior. Neuropsychologia *50*, 435–446.
13. Haynes, J.D., and Rees, G. (2006). Decoding mental states from brain activity in humans. Nat. Rev. Neurosci. *7*, 523–534.
14. Kamitani, Y., and Tong, F. (2006). Decoding seen and attended motion directions from activity in the human visual cortex. Curr. Biol. *16*, 1096–1102.
15. Haynes, J.D., and Rees, G. (2005). Predicting the orientation of invisible stimuli from activity in human primary visual cortex. Nat. Neurosci. *8*, 686–691.
16. Vanduffel, W., Tootell, R.B., Schoups, A.A., and Orban, G.A. (2002). The organization of orientation selectivity throughout macaque visual cortex. Cereb. Cortex *12*, 647–662.
17. Freeman, J., Brouwer, G.J., Heeger, D.J., and Merriam, E.P. (2011). Orientation decoding depends on maps, not columns. J. Neurosci. *31*, 4792–4804.
18. Norman, K.A., Polyn, S.M., Detre, G.J., and Haxby, J.V. (2006). Beyond mind-reading: multi-voxel pattern analysis of fMRI data. Trends Cogn. Sci. *10*, 424–430.
19. Hubel, D.H., and Wiesel, T.N. (1963). Shape and arrangement of columns in cat's striate cortex. J. Physiol. *165*, 559–568.
20. Blasdel, G.G., and Salama, G. (1986). Voltage-sensitive dyes reveal a modular organization in monkey striate cortex. Nature *321*, 579–585.
21. Miyawaki, Y., Uchida, H., Yamashita, O., Sato, M.A., Morito, Y., Tanabe, H.C., Sadato, N., and Kamitani, Y. (2008). Visual image reconstruction from human brain activity using a combination of multiscale local image decoders. Neuron *60*, 915–929.
22. Brouwer, G.J., and Heeger, D.J. (2009). Decoding and reconstructing color from responses in human visual cortex. J. Neurosci. *29*, 13992–14003.
23. Kay, K.N., Naselaris, T., Prenger, R.J., and Gallant, J.L. (2008). Identifying natural images from human brain activity. Nature *452*, 352–355.
24. Scolari, M., Byers, A., and Serences, J.T. (2012). Optimal deployment of attentional gain during fine discriminations. J. Neurosci. *32*, 7723–7733.
25. Regan, D. (1989). Human Brain Electrophysiology: Evoked Potentials and Evoked Magnetic Fields in Science and Medicine (New York: Elsevier).
26. Ho, T., Brown, S., van Maanen, L., Forstmann, B.U., Wagenmakers, E.J., and Serences, J.T. (2012). The optimality of sensory processing during the speed-accuracy tradeoff. J. Neurosci. *32*, 7992–8003.
27. Scolari, M., and Serences, J.T. (2009). Adaptive allocation of attentional gain. J. Neurosci. *29*, 11933–11942.
28. Busse, L., Katzner, S., and Treue, S. (2008). Temporal dynamics of neuronal modulation during exogenous and endogenous shifts of visual attention in macaque area MT. Proc. Natl. Acad. Sci. USA *105*, 16380–16385.
29. Mirabella, G., Bertini, G., Samengo, I., Kilavik, B.E., Frilli, D., Della Libera, C., and Chelazzi, L. (2007). Neurons in area V4 of the macaque translate attended visual features into behaviorally relevant categories. Neuron *54*, 303–318.
30. Chen, X., Hoffmann, K.P., Albright, T.D., and Thiele, A. (2012). Effect of feature-selective attention on neuronal responses in macaque area MT. J. Neurophysiol. *107*, 1530–1543.
31. Kaneoke, Y., Urakawa, T., and Kakigi, R. (2009). Visual motion direction is represented in population-level neural response as measured by magnetoencephalography. Neuroscience *160*, 676–687.
32. Regan, D., and Regan, M.P. (1987). Nonlinearity in human visual responses to two-dimensional patterns, and a limitation of Fourier methods. Vision Res. *27*, 2181–2183.
33. Pouget, A., Dayan, P., and Zemel, R.S. (2003). Inference and computation with population codes. Annu. Rev. Neurosci. *26*, 381–410.
34. McAdams, C.J., and Maunsell, J.H. (1999). Effects of attention on orientation-tuning functions of single neurons in macaque cortical area V4. J. Neurosci. *19*, 431–441.
35. Treue, S., and Martínez Trujillo, J.C. (1999). Feature-based attention influences motion processing gain in macaque visual cortex. Nature *399*, 575–579.

36. Saproo, S., and Serences, J.T. (2010). Spatial attention improves the quality of population codes in human visual cortex. J. Neurophysiol. *104*, 885–895.
37. Buracas, G.T., and Boynton, G.M. (2007). The effect of spatial attention on contrast response functions in human visual cortex. J. Neurosci. *27*, 93–97.
38. Pestilli, F., Carrasco, M., Heeger, D.J., and Gardner, J.L. (2011). Attentional enhancement via selection and pooling of early sensory responses in human visual cortex. Neuron *72*, 832–846.
39. Breakspear, M., Heitmann, S., and Daffertshofer, A. (2010). Generative models of cortical oscillations: neurobiological implications of the kuramoto model. Front Hum Neurosci *4*, 190.
40. Bridwell, D.A., and Srinivasan, R. (2012). Distinct attention networks for feature enhancement and suppression in vision. Psychol. Sci. *23*, 1151–1158.
41. Swisher, J.D., Gatenby, J.C., Gore, J.C., Wolfe, B.A., Moon, C.H., Kim, S.G., and Tong, F. (2010). Multiscale pattern analysis of orientation-selective activity in the primary visual cortex. J. Neurosci. *30*, 325–330.
42. Vialatte, F.B., Maurice, M., Dauwels, J., and Cichocki, A. (2010). Steady-state visually evoked potentials: focus on essential paradigms and future perspectives. Prog. Neurobiol. *90*, 418–438.
43. Nunez, P.L., and Cutillo, B.A. (1995). Neocortical Dynamics and Human EEG Rhythms (New York: Oxford University Press).